Journal of Structural Geology 31 (2009) 1223–1237

Contents lists available at ScienceDirect

Journal of Structural Geology

journal homepage: www.elsevier.com/locate/jsg

Influence of melt induced mechanical anisotropy on the magnetic fabrics and rheology of deforming migmatites, Central Vosges, France

Karel Schulmann [a], Jean-Bernard Edel [a], Pavlína Hasalová [b,*], John Cosgrove [c], Josef Ježek [d], Ondrej Lexa [d]

[a] L'Université de Strasbourg, l'Institut de Physique du Globe de Strasbourg, UMR 7516, 1 rue Blessig, Strasbourg 67084, France
[b] School of Geosciences, Monash University, Clayton, Victoria 3800, Australia
[c] Department of Earth Science and Engineering, Royal School of Mines, Imperial College of Science, Technology & Medicine, Prince Consort Rd, London SW7 2AZ, UK
[d] Institute of Petrology and Structural Geology, Faculty of Science, Charles University, Albertov 6, 12843, Prague, Czech Republic

ARTICLE INFO

Article history:
Received 17 February 2008
Received in revised form
16 June 2009
Accepted 3 July 2009
Available online 16 July 2009

Keywords:
AMS
Fabric modeling
Melt
Migmatites
Migmatite rheology
Vosges

ABSTRACT

In the Central Vosges (France), we describe and model the structural relationships existing between orthogneiss domains and their surrounding viscous migmatites. These domains show a structural and anisotropy of magnetic susceptibility (AMS) zonation associated with an increasing amount of melt from the core to their margins. A pre-extension oblate to plane strain fabric is preserved in the core of the orthogneiss domains where the granite veins were emplaced along a dilated mechanical anisotropy. The internal margin of the orthogneiss bodies exhibits development of a prolate fabric and active buckling of an orthogneiss/granite multilayer. The external margin of the orthogneiss bodies is characterized by oblate fabrics resulting from a layer perpendicular shortening of a melt-orthogneiss multilayer, pinch-and-swell structures and extensional kink bands along which granite veins have been injected. The surrounding metasedimentary migmatites show a similar structural history but the degree of fabric resetting is significantly higher. This systematic fabric and structural succession is due to contrasting rheological evolution between orthogneiss and metasedimentary migmatites during progressive melting and continuously evolving degree of mechanical anisotropy in the stronger orthogneiss. Numerical modeling confirms the role of the relationship between initial mechanical anisotropy and superimposed deformation overprints on finite AMS fabrics in migmatites.

1. Introduction

Anisotropy of magnetic susceptibility (AMS) is a popular petrophysical method allowing quantification of various fabric parameters in magmatic (e.g. Bouchez, 1997) and metamorphic rocks (e.g. Borradaile and Henry, 1997). So far AMS was mostly used to provide orientation data such as magnetic foliation and lineation which are commonly correlated with sedimentary, magmatic and deformation structures (e.g. Bouchez, 1997). Modern AMS studies show systematic relationships between strain, metamorphic degree, lithologies, magnetic susceptibility and fabric (Borradaile and Jackson, 2004). In addition, variations of fabric symmetry and intensity can arise from complex deformation history like superposition of cleavage on sedimentary fabrics and folding (Hrouda, 1991; Parés and Van der Pluijm, 2003; Debacker et al., 2004). This relationship between intensity and shape of the magnetic susceptibility ellipsoid and complex deformation overprints in some rocks is confirmed by numerical fabric modeling (Housen et al., 1993; Benn, 1994).

Migmatites, because of their complexity, have been studied only rarely using the AMS method which concentrated either on methodological approaches (Ferré et al., 2003) or solution of basic tectonic questions (e.g. Egydio-Silva et al., 2005). The main problem of migmatites is the imprecisely defined transition between mechanical behaviors of weakly molten rocks (metatexites) and rocks with high melt proportion (diatexites). Brown et al. (1995) discussed the transition from metatexites marked by a pervasive flow of melt through a network of foliation-parallel veins, to melt-dominated diatexites, marked by the disruption of a solid network and development of true magmatic flow in granitic rocks. These authors emphasized that in nature it is almost impossible to draw a line between a solid network intruded by granitic veins and gneissic enclaves transported by a viscous melt. Vanderhaeghe (1999) suggested that in fertile metapelites the melt fraction may

* Corresponding author. School of Geosciences, Monash University, Clayton, Victoria 3800, Australia. Tel.: +61 (0) 3 99051142; fax: +61 (0) 3 99054903.
E-mail address: hasalovap@gmail.com (P. Hasalová).

0191-8141/$ – see front matter © 2009 Elsevier Ltd. All rights reserved.
doi:10.1016/j.jsg.2009.07.004

form a diffuse network of foliation-parallel veins. In contrast, in the refractory lithologies the melt fraction migrated through a network of fractures using mechanically weak foliation planes or along fractures oriented at high angle to the main planar anisotropy. This example emphasizes a qualitative difference between rheological properties of hot country rocks that involve a ductily deforming matrix and the formation of foliation-parallel veins. However, there is no quantitative structural study which examines the relationship between degree of partial melting and the mechanical behavior of solids and melts during deformation.

The anisotropy of magnetic susceptibility (AMS) can be used to address this problem, representing a well-suited method that describes various fabric parameters in both the migmatitic veins and the host rock (Ferré et al., 2003). However, the interpretation of the AMS fabrics in migmatites is possible only if the fabric of the solid state rocks is distinguished from that of granite veins, and if the carriers of magnetic anisotropy are known.

The migmatites of the Vosges Mountains (France) offer an adequate example of a crustal section of partially molten crust. There, the structural relationships between a variety of migmatites and adjacent granites were studied together with their AMS fabrics which were found to correlate with melt proportion and intensity of the bulk deformation. These data are used to discuss the role of the mechanical anisotropy in the solid rock, the proportion of granite melt and the viscosity contrast between the different types of host rocks and granite veins on the rheology and deformation of these rocks. Finally, the role of the relationship between initial mechanical anisotropy and superimposed deformation overprints is simulated by means of AMS fabric modeling.

2. Geological setting

The Vosges Mountains in eastern France represents an isolated and relatively small outcrop of the European Variscan orogenic belt. It contains a crystalline core consisting of high grade rocks in the north and migmatites associated with crustal granitoids in the central part of the chain (Fig. 1a). The metamorphism and magmatism are of Carboniferous age and occurred during two major stages. The first one is characterized by development of granulite ($T = \sim 750\,^{\circ}C$, $P = 9$–11 kbar; Rey et al., 1992) and amphibolite facies rocks ($T = \sim 650\,^{\circ}C$, $P = 6$ kbar; Latouche et al., 1992). This event is dated at ~335 Ma (U–Pb zircon; Schaltegger et al., 1999) and granulite polyphase fabrics are interpreted as a result of crustal thickening (Schulmann et al., 2002) followed by vertical extrusion of lower crustal rocks over mid-crustal schists and gneisses (Kratinová et al., 2007). The second extensional event occurred in amphibolites facies conditions ($\sim 700\,^{\circ}C$, $P = 3$ kbar; Rey et al., 1992) and is characterized by pervasive anatexis and intrusion of voluminous anatectic granites dated at ~325 Ma (U–Pb zircon; Schaltegger et al., 1999).

3. Petrography and microstructures of the principal rock types

The studied migmatitic complex (Fig. 1b, c) consists of two main rock types: (i) metasedimentary migmatites connected to variable proportions of anatectic granites surrounding (ii) two orthogneiss domains.

Metasedimentary migmatites occur in the eastern and western parts of the studied area (Fig. 1b, c) and can be divided in two types: metatexites and diatexites (Fig. 2a). The *metatexite* (20–30% of former melt; Table 1) is a medium to coarse grained rock consisting of plagioclase, less abundant K-feldspar, quartz, biotite and muscovite. Zircon, monazite, magnetite and titanomagnetite are present as accessory phases (<1%). The mineral assemblage of *diatexite* (30–80% of former melt; Table 1) is plagioclase, K-feldspar, quartz, biotite, muscovite with accessory amount of zircon, monazite, magnetite and titanomagnetite. The diatexites (Fig. 3a) show idiomorphic plagioclase and K-feldspar indicating crystallization from melt. The migmatites are associated with medium grained *anatectic granite* (>80% of former melt; Table 1), locally porphyritic (Fig. 2b). In the anatectic granite the fabric is underlined by a weak alignment of biotite and by a shape-preferred orientation of K-feldspar phenocrysts. Locally, boudins of restitic *metagraywackes* (<10% of former melt; Table 1) occur (Fig. 2b).

Orthogneisses can be divided in two groups: orthogneiss and migmatitic orthogneiss (Fig. 2c & Table 1). The statically recrystallized *orthogneiss* with low melt fraction (<10% of former melt; Table 1) is characterized by fine-grained plagioclase, quartz and K-feldspar matrix (Fig. 3b) with minor biotite, muscovite and garnet and accessory apatite, zircon and monazite. Plagioclase, K-feldspar and quartz show irregular shapes with straight to slightly lobate boundaries. Plagioclase grains display normal zoning with andesine cores (An_{30-50}) and thin distinct albite/oligoclase rims (An_{10-18}). Biotite (Ti = 0.12–0.16 p.f.u., $X_{Mg} = 0.32$–0.36) is arranged into irregular elongate aggregates with a strong preferred orientation (Fig. 3e). Poikilitic garnets are partially replaced by biotite. This orthogneiss is interlayered with a more isotropic *migmatitic orthogneiss* (Fig. 2c) that contains relatively high melt fraction (10–30% of former melt; Table 1) and its typical mineral assemblage is plagioclase, K-feldspar, quartz, biotite and muscovite. The K-feldspar and plagioclase form irregular corroded grains with highly lobate boundaries overgrown with newly crystallized feldspars and quartz and myrmekites (Fig. 3c). Quartz occurs in large grains with highly lobate boundaries (Fig. 3c). Zircon, monazite, apatite, titanomagnetite and rutile are present as accessory phases (Fig. 3d). Biotite (Ti = 0.15–0.18 p.f.u., $X_{Mg} = 0.4$–0.45) is evenly dispersed in an equigranular matrix and shows strongly corroded shapes (Fig. 3f). In several places both orthogneiss types are cross-cut by *leucogranite* and *anatectic granite* dykes with highly variable orientations with respect to host rock fabric (Fig. 2d).

4. Macroscopic structures versus melt proportions

The migmatite complex represents a relatively voluminous portion of formerly partially molten crust immersed in the anatectic granites which show W- to SW-dipping magmatic foliation and S- to SSE-plunging mineral lineation (Fig. 1b, c). The structural evolution is characterized by two main fabric-forming events. The early deformation D_1 is represented by solid state deformation fabrics well preserved in the orthogneiss and locally also in the metasedimentary migmatites. These early structures are reworked by a sub-horizontal D_2 fabric associated with a subsequent extensional deformation and extensive melting (Rey et al., 1992; Kratinová et al., 2007).

4.1. Metasedimentary migmatites and associated anatectic granites

The planar fabric of the meta- and diatexites is formed by migmatite layering and a preferred orientation of dispersed biotite. The rarely preserved S_1 foliation in the metatexites is folded by decimetre to metre scale F_2 folds (Fig. 2a). The leucosomes are commonly located in fold hinge regions or parallel to the mesosome foliation. In highly molten regions, the enclaves of folded metatexites and metagraywackes are concordant with the dominant S_2 fabric of the surrounding diatexites and anatectic granites (Fig. 2b). Locally, a transition from magmatic to sub-magmatic and up to solid state deformation was observed leading to the development of C/S structures indicating a top to the SSE movement. In

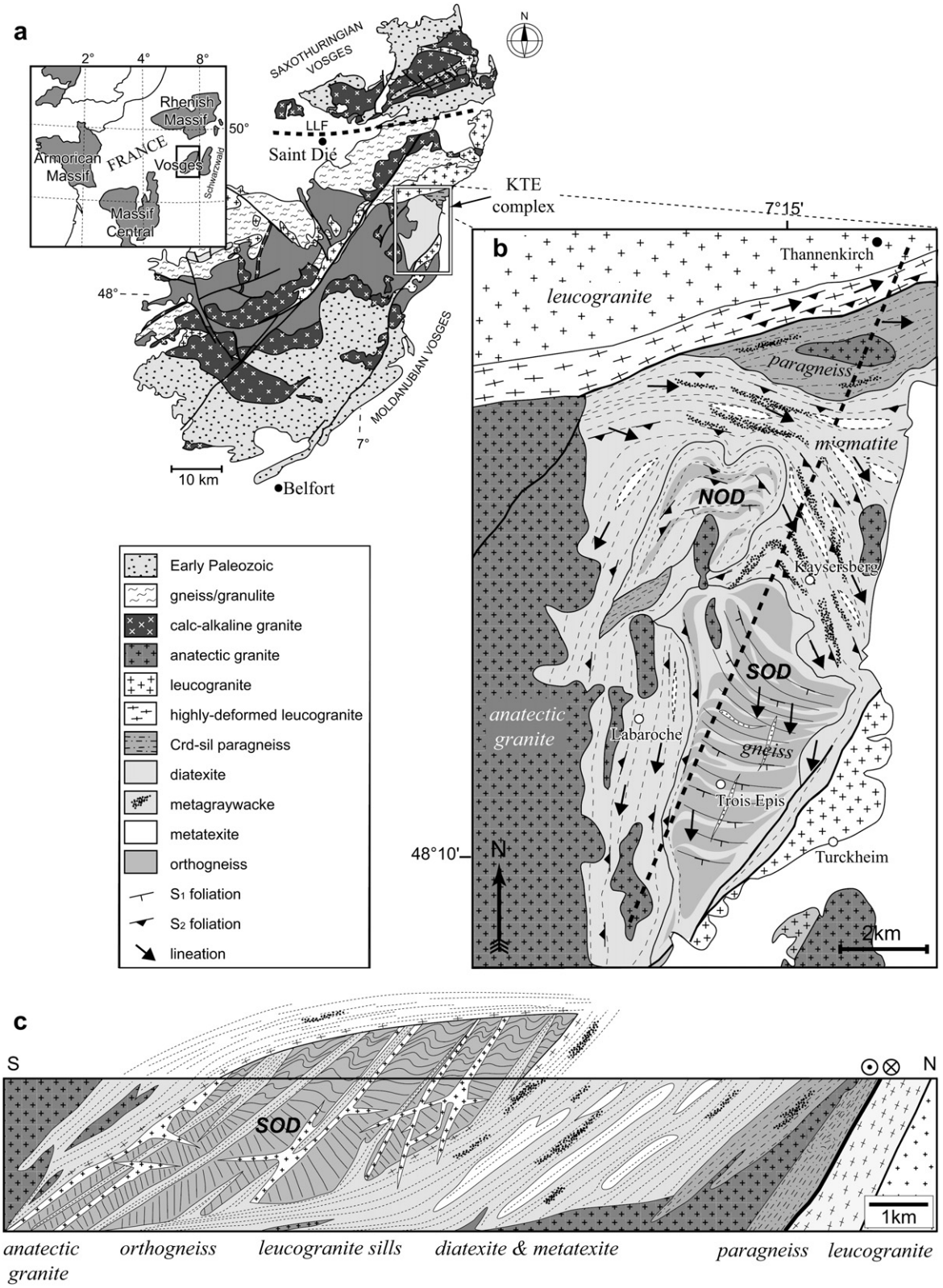

Fig. 1. (a) Simplified geological map of the Vosges with the location of the study area (white rectangle). (b) Detailed map of the migmatitic complex in the southern Vosges. The black dashed line corresponds to the location of the cross-section. NOD = North Orthogneiss Domain; SOD = South Orthogneiss Domain. (c) Schematic N-S cross-section through the migmatitic complex. Vertical axis not to scale.

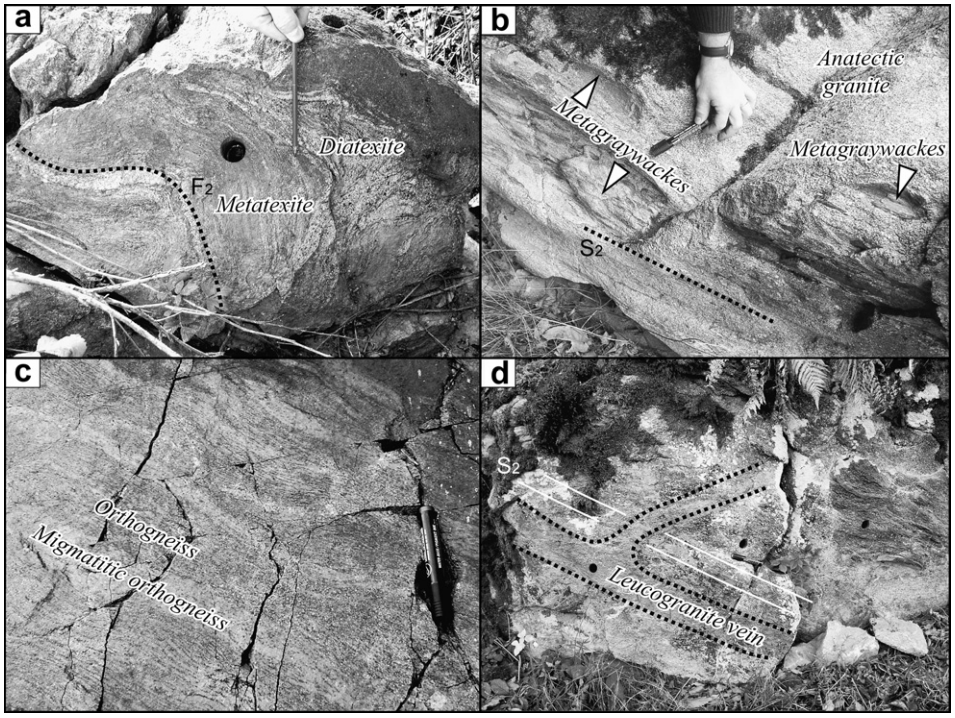

Fig. 2. Field photographs illustrating the main rock types in the study area and their structural characteristics. (a) Disharmonically folded biotite-rich meta- and diatexite. (b) Heterogeneous enclaves of gneisses and metagreywackes arranged parallel to the magmatic fabric of the surrounding anatectic granite (black dashed line). (c) Alternation of the orthogneiss and migmatitic orthogneiss in an outcrop scale. (f) Leucogranite vein (black dashed lines) cross-cutting migmatites.

this case, the S_2 foliation contains a strong stretching lineation plunging to the SSE. The diatexites and associated anatectic granite show a less pronounced mineral lineation. In these rocks the regional stretching direction is defined by elongate ellipsoidal boudins of metagraywackes which are elongated parallel to the SSE trending L_2 mineral lineation.

4.2. South and north orthogneiss domains

Two orthogneiss bodies represent large scale anisotropic boudins surrounded by metasedimentary migmatites and anatectic granites. The structural relationships between both boudins and surrounding rocks are shown in the schematic model (Fig. 4).

4.2.1. South orthogneiss domain (SOD)

This NE–SW elongated orthogneiss domain (SOD) is surrounded by metasedimentary migmatites to the east and anatectic granites to the west (Fig. 1b). In order to quantify the relationship between deformation and melt proportion, amount of former melt in individual outcrops based on macroscopic and microscopic observations was estimated. This analysis shows that the SOD can be divided into three zones according to proportion of former melt (Figs. 4 and 5): (A) *the central zone*, 3 km wide made of ~10–30% of former melt; (B) *the internal margin*, up to 1 km wide, made of ~30–50% of former melt; and (C) a narrow 0.5–1 km wide *external margin* characterized by 50–80% of former melt. Accordingly, the amount of melt is systematically increasing from east to the west and from north to the south (Fig. 5). Moreover, the central zone of SOD consist of 80% of orthogneiss and 20% of migmatitic orthogneiss, while the percentage of migmatitic orthogneiss increases up to 40% in the internal marginal zone and up to 70% in the external marginal zone.

The general structure of the orthogneiss domain is characterized by dominant layer parallel gneissosity S_1 formed by arrangement of planar biotite aggregates (Fig. 2c). The S_1 is steeply dipping to the south or to the southwest in central part of the SOD (Figs. 1 and 4). In some places leucogranite veins without any apparent internal fabric intrude sub-parallel to the S_1 foliation of the host rock or occasionally cross-cut the orthogneisses at a high angle to the foliation (Fig. 4). In the internal margin of the SOD (B in Fig. 4) the S_1 foliation dips either to the south or to the west at medium to steep angles thus forming large scale asymmetrical folds. The fabric of the orthogneiss is cross-cut by zones of migmatitic orthogneiss, which are either parallel to or at high angle to the S_1 fabric of the host rock. The westerly dipping layers of both orthogneisses are interlayered with and/or cross-cut by leucogranitic veins several decimetres to

Table 1
Mineral assemblages and melt proportions in present lithologies.

	Rock type	Mineral assemblage	Melt % in the rock
Metasedimentary migmatites and associated granites	*Metagraywacke*	Pl + Kfs + Qtz + Bt ± Mag ± Ti-Mag	<10%
	Metatexite	Pl + Kfs + Qtz + Bt + Ms ± Zrn ± Mnz ± Ap ± Ti-Mag	20–30%
	Diatexite	Pl + Kfs + Qtz + Bt + Ms ± Zrn ± Mnz ± Ap ± Mag ± Ti-Mag	30–80%
	Anatectic granite	Pl + Kfs + Qtz + Bt + Ms ± Mag ± Ilm	>80%
	Leucogranite	Pl + Kfs + Qtz + Bt + Ms ± Zrn ± Mag	100%
Orthogneiss/migmatites	*Orthogneiss*	Pl + Kfs + Qtz + Bt + Ms ± Grt ± Zrn ± Mnz ± Ap	~10%
	Migmatitic orthogneiss	Pl + Kfs + Qtz + Bt ± Ms ± Zrn ± Mnz ± Ap ± Ti-Mag ± Rt	10–30%

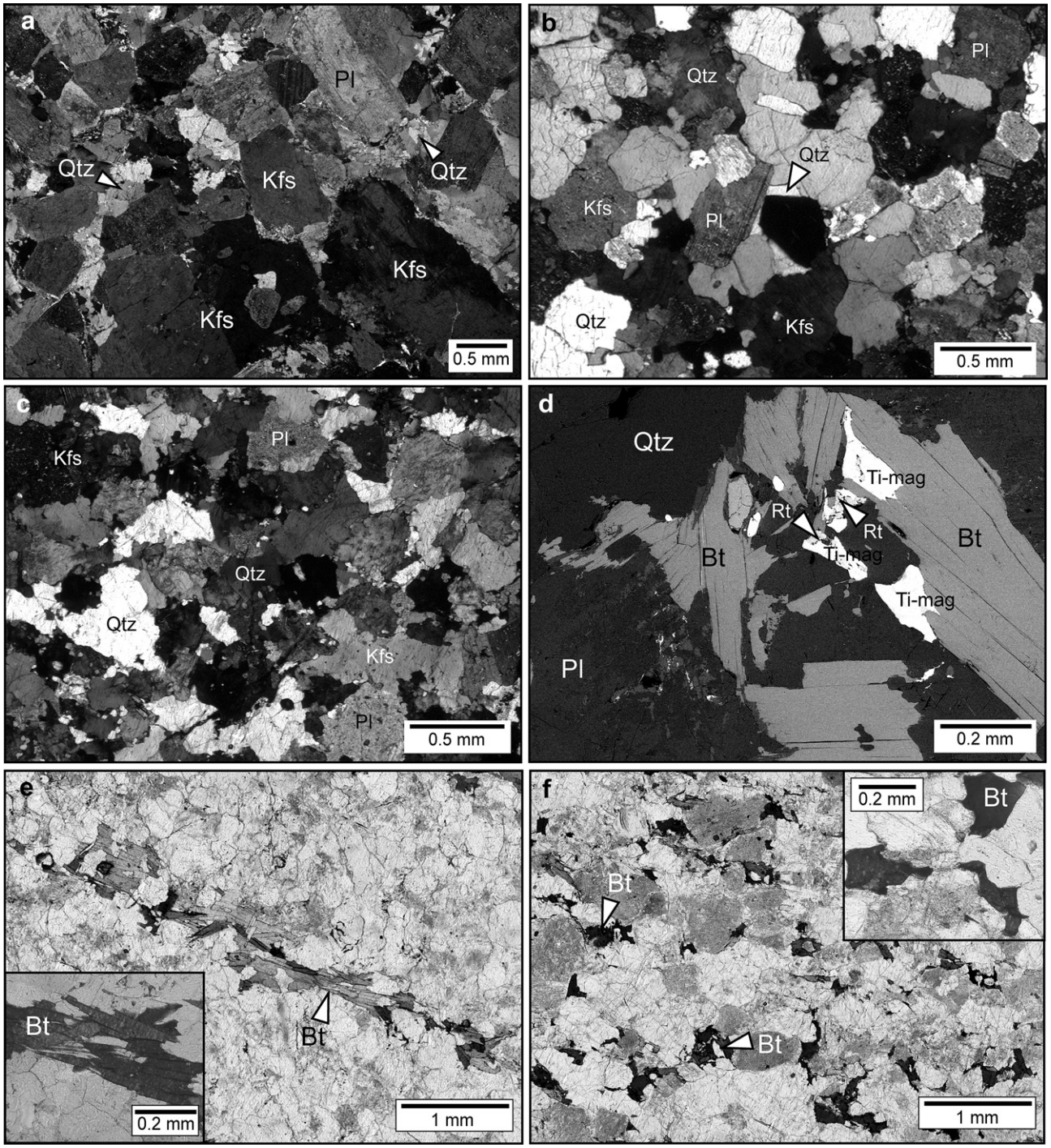

Fig. 3. Principal microtextures of the rock types. (a) Diatexite showing the idiomorphic shapes of plagioclase and K-feldspars and incipient recrystallization of quartz (white arrow). (b) Orthogneiss showing an equilibrated mosaic of feldspars and quartz and interstitial feldspars and quartz (white arrow). (c) Migmatitic orthogneiss composed of irregular corroded feldspars traced out by newly crystallized interstitial feldspars and quartz grains. (d) BSE image of typical titanomagnetite appearance in migmatitic orthogneiss. (e) Biotite aligned into elongate aggregates with a strong preferred orientation. Inset shows decussate biotite structure. (f) Dispersed biotite in a migmatitic orthogneiss. Inset show biotite with corroded shapes.

metres in width. Further to the west, in the external margin of the SOD (C in Fig. 4), the layers of orthogneisses are parallel to the magmatic fabric of thick granite veins (Fig. 4).

4.2.2. North orthogneiss domain (NOD)

The centre of the north orthogneiss domain is characterized by 30–50% of former melt (equivalent to the internal margin of the SOD), whilst most of the NOD surface exhibits 50–80% of former melt corresponding to the external margin of the SOD (Fig. 5). The S_1 foliation is preserved only locally in orthogneiss sheets and is parallel to the dominant S_2 fabric of surrounding diatexites and granites (Fig. 4). This composite S_{1-2} foliation dips mostly to the south and southwest at a gentle to medium angle (Figs. 1 and 4). In some places, the compositional layering formed by sheets of

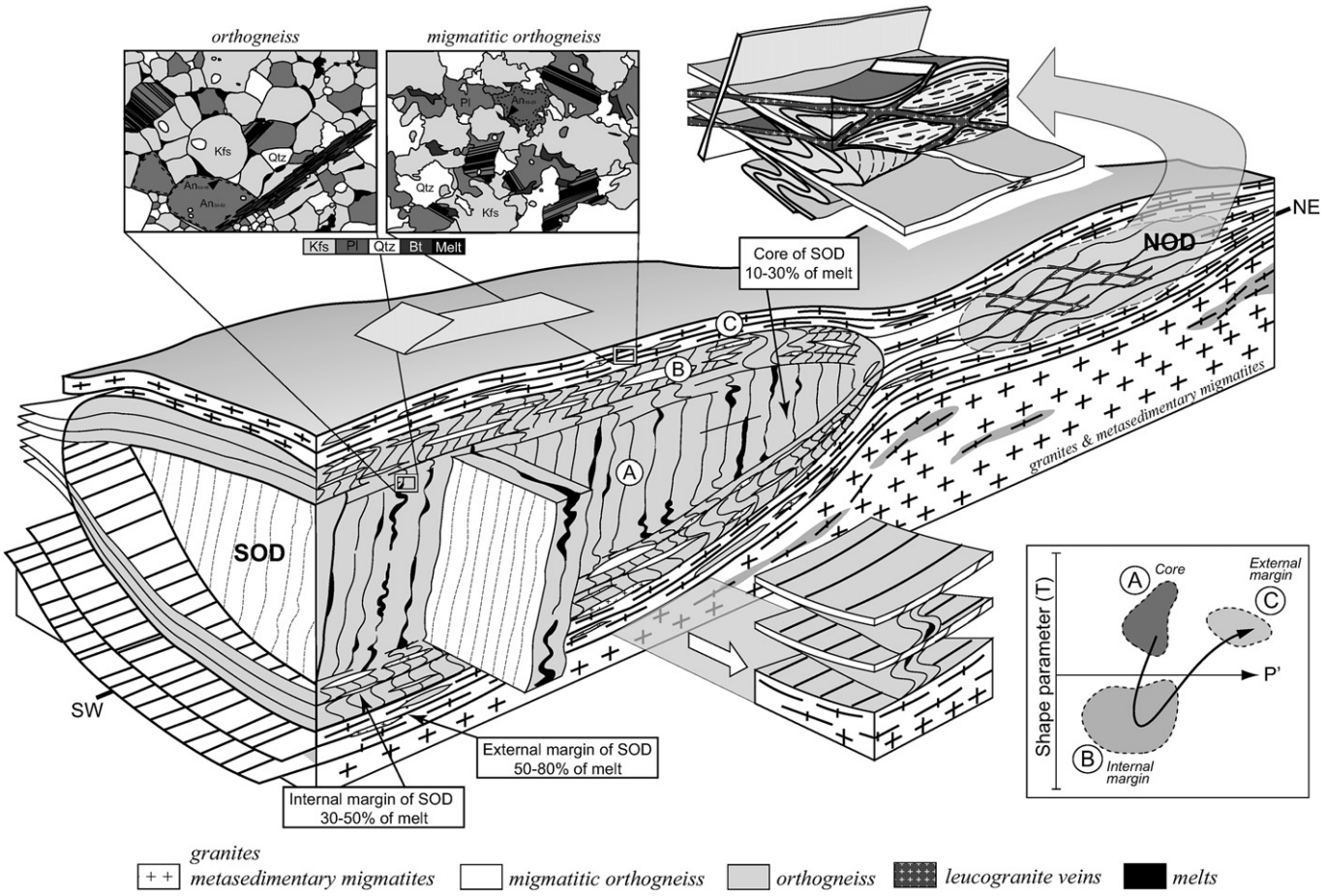

Fig. 4. Schematic representation of orthogneiss domains surrounded by the migmatites and anatectic granites. The central domain (A) suffers layer parallel D_2 dilation. The internal margin of the SOD (B) shows buckling of the orthogneiss/melt multilayer (detail given in the small block diagram); the external margin of the SOD (C) exhibits structures compatible with layer perpendicular shortening. The significantly more deformed NOD with a well developed S_2 fabric accompanied by shear bands filled by leucogranites is shown in an enlarged inset. The lower right inset displays the evolution of anisotropy of magnetic susceptibility (expressed by P′ versus T) in the different parts of the migmatitic complex. The upper left inset shows microstructural appearance of both orthogneisses types.

orthogneiss, migmatitic orthogneiss and granites is cross-cut by conjugate set of leucogranite veins (Fig. 2d). Locally, large granitic veins cross-cut interlayered orthogneiss and granite at a high angle to the foliation.

5. Magnetic fabrics

In order to propose a consistent model of (i) melt behavior with respect to the solid network of the host and (ii) relationship between magma flow and deformation of solid enclaves, a detailed fabric characterization is needed. For this reason, we carried out an AMS study of the main lithologies with variable proportions of melt.

5.1. Sampling strategy and magnetic measurements

Measurement of the bulk magnetic susceptibility and of the anisotropy of magnetic susceptibility was performed on 1321 specimens (2.5 cm diameter, 2.25 cm length) from 108 sites distributed regularly in the whole migmatitic complex and the adjacent granites. For the purpose of the AMS study meta- and diatexites, orthogneisses, anatectic granites and leucogranites were evaluated separately. The statistical processing and evaluation was carried out using the ANISOFT programs (Jelínek, 1978). The magnetic susceptibility and anisotropy were measured with AGICO instruments. Susceptibility versus temperature variations was obtained using a CS-3 apparatus and a KLY-3S Kappabridge.

There is a fairly developed trend in increasing average susceptibility (K_m) from leucogranite via orthogneisses to meta- and diatexite (Fig. 6a). The leucogranite is characterized by the weakest susceptibilities ($K_m = 88 \times 10^{-6}$ SI, $\sigma = 61 \times 10^{-6}$; Fig. 6a) and the K/t thermomagnetic curve (Fig. 6b) reveals the coexistence of paramagnetic minerals and scarce magnetite that is characterized by a drop of the susceptibility around 580 °C.

Both orthogneiss and migmatitic orthogneiss show similar distribution of susceptibilities as the leucogranite with a slightly higher mean ($K_m = 103 \times 10^{-6}$ SI, $\sigma = 35 \times 10^{-6}$; Fig. 6a). The K/t thermomagnetic curves indicate that paramagnetic minerals, specifically biotite, are the main carriers of the magnetization (Fig. 6b). However the mean intensity of Natural Remanent Magnetization (NRM) of 9×10^{-4} Am^{-1} indicates that some ferromagnetic minerals are also present. For the orthogneiss the mean NRM is slightly lower i.e. 5.5×10^{-4} Am^{-1} compared to migmatitic orthogneiss. In the orthogneiss the thermal demagnetization of the normalized NRM J/t curves mostly show a decrease in the range 320–400 °C (Fig. 6c), which suggests minor presence of titanomagnetite, pyrrhotite or maghemite. This is compatible with a small drop of the susceptibility in the range of 300–350° on K/t curves of these rocks (Fig. 6b). Above these temperatures the remanence and the susceptibility increase which is due to the formation of magnetite during heating. In one case the thermomagnetic curves indicate hematite as carrier of the induced and remanent magnetizations in orthogneiss.

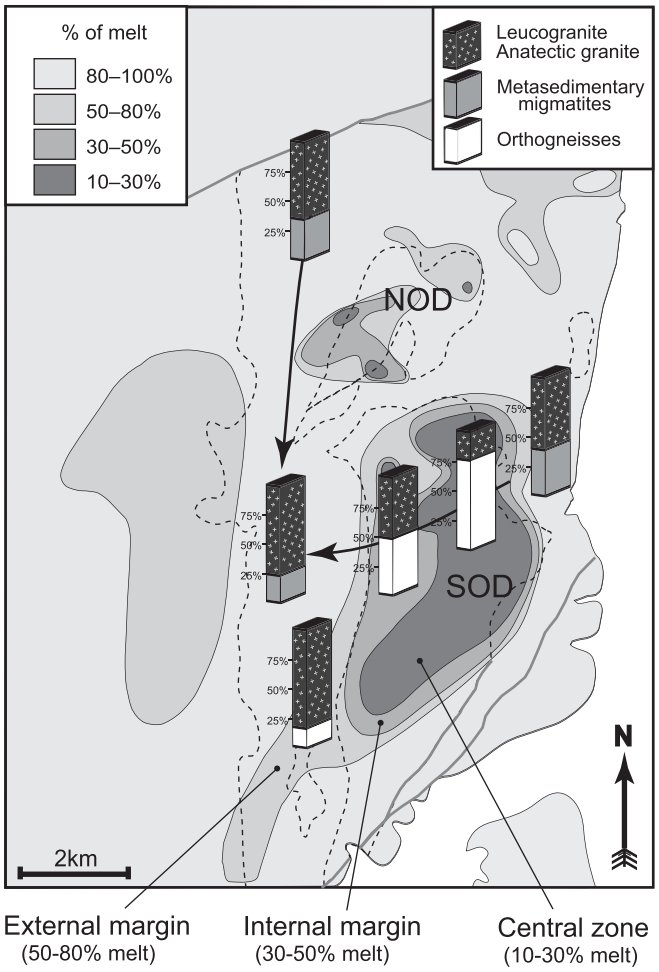

Fig. 5. Synoptic map of the studied area showing the melt proportions within both orthogneiss domains (SOD and NOD) and the surrounding metasedimentary migmatites. The histograms with proportions of individual lithologies are presented for different parts of the studied area. Note increasing amount of melt from east to the west and from north to the south.

In contrast, the K/t and J/t curves of migmatitic orthogneiss (Fig. 6b,c) show higher Curie temperatures in the range from 480° to 580 °C indicating a presence of magnetite corroborating the appearance of titanomagnetite determined by SEM (Fig. 3d).

Anatectic granites and diatexites display high susceptibilities with $K_m = 152 \times 10^{-6}$ and $\sigma = 53 \times 10^{-6}$ (Fig. 6a) which, according to the thermomagnetic curves, is due to the coexistence of paramagnetic biotite with a weak amount of ferromagnetic minerals (Fig. 6b). The drop of J/t curves in the range 320–400° or 580° indicates that these minerals can be titanomagnetite, sulphides or magnetite. The metatexites show the highest bulk susceptibility ($K_m = 242 \times 10^{-6}$, $\sigma = 65 \times 10^{-6}$; Fig. 6a) and the thermomagnetic curves indicate high amounts of biotite as well as significant presence of magnetite (Fig. 6b). In these rocks the intensity of NRM exceeds 20×10^{-4} Am^{-1} (Fig. 6c).

This magnetic mineralogy study is consistent with the microscopically determined presence of Ti-rich biotite (10–15%) in orthogneiss. SEM and microprobe study of migmatitic orthogneiss reveals intergrowths of partly resorbed biotite (5–10%) with new titanomagnetite, locally associated with rutile (Fig. 3d). Magnetic mineralogy also confirms the presence of common magnetite and titanomagnetite in anatectic granite and metasedimentary migmatites.

5.2. Magnetic fabric of the metasedimentary migmatites and anatectic granites

The magnetic fabric trajectories (Fig. 7) exhibit consistent fabric patterns: the foliations dip gently to the southwest in the east and at a moderate to steep angle in the west and the magnetic lineations are sub-horizontal and oriented NNW-SSE. This trend changes into E–W in the northern part of the area. The degree of AMS expressed by the P' parameter (Jelínek, 1981; $P' = \exp\sqrt{[(\ln K_1 - \ln K_m)^2 + (\ln K_2 - \ln K_m)^2 + (\ln K_3 - \ln K_m)^2]}$) is generally low ($P' = 1$–1.08) in the diatexites, anatectic granites and leucogranites, and the shape ellipsoid of these rocks is mostly prolate to oblate (Fig. 7). As a rule the metatexites yield higher anisotropy degrees ($P' = 1.05$–1.1) and have more oblate magnetic ellipsoids compared to diatexites. The more competent metagraywackes show the same magnetic fabric as surrounding diatexites and granites but show highest degree of magnetic susceptibility and the most oblate shapes of AMS ellipsoid from all studied rocks (Fig. 7).

5.3. Magnetic fabric of the SOD and NOD orthogneiss bodies

The foliations of the orthogneiss in the centre of the SOD are generally dipping to the SSW or SW at steep to gentle angles and contain magnetic lineations plunging to the SSW at variable angles (Fig. 8). Their degree of anisotropy is rather low ($P' = 1.03$–1.08) and the shape of their fabric ellipsoids varies from oblate to plane. The leucogranite veins show magnetic foliation sub-parallel to that of surrounding orthogneiss and sub-horizontal magnetic lineation plunging to the SSW.

At the internal margin of the SOD, the orthogneiss shows magnetic foliations dipping either to the S or to the W defining a broad girdle (Fig. 8). The magnetic lineation forms also a broad girdle with steep to moderate plunges ranging from the west to the SSW. The magnetic ellipsoids of the orthogneiss have predominantly prolate shapes and weak anisotropy degrees ($P' = 1.01$–1.08). Rare orthogneiss samples with strongly oblate shapes show orientations characteristic for the central zone of the SOD (dark grey symbols in Fig. 8B). The magnetic foliations of the migmatitic orthogneiss dip to the W or SW and carry a sub-horizontal and S plunging magnetic lineation. Their degree of anisotropy is rather low ($P' = 1.03$–1.06) along with plane strain to prolate magnetic ellipsoids (Fig. 8).

In the external margin of the SOD the magnetic foliations of both orthogneisses dip to the SW and W. The magnetic lineation shows plunges that progressively evolve towards the SSW direction typical for adjacent diatexites and anatectic granites (Figs. 7 and 8). The magnetic ellipsoid is weakly prolate to oblate with degree of magnetic susceptibility higher compared to internal margin of the SOD ($P' = 1.04$–1.1). The migmatitic orthogneiss layers show magnetic fabric parallel to S_2 foliation in adjacent anatectic granite and exhibit dominantly prolate shape of AMS ellipsoid (Figs. 7 and 8). Granite veins cross-cutting well aligned orthogneiss and anatectic granite layering show steep E–W or N–S trending magnetic foliation and vertical magnetic lineation (Fig. 8).

In the NOD, both orthogneisses displays magnetic foliations dipping to the S or to the W at moderate to steep angles and is coherent with that of the surrounding granites (Figs. 7 and 8). The magnetic lineations of the migmatitic orthogneiss form a southeast plunging maximum sub-parallel to the regional lineation (Fig. 7) compared to orthogneiss that shows a larger spread of lineations (Fig. 8). The shapes of the fabric ellipsoids of the orthogneiss are oblate with a stronger degree of anisotropy ($P' = 1.02$–1.11) compared to orthogneiss samples of the centre and internal margin

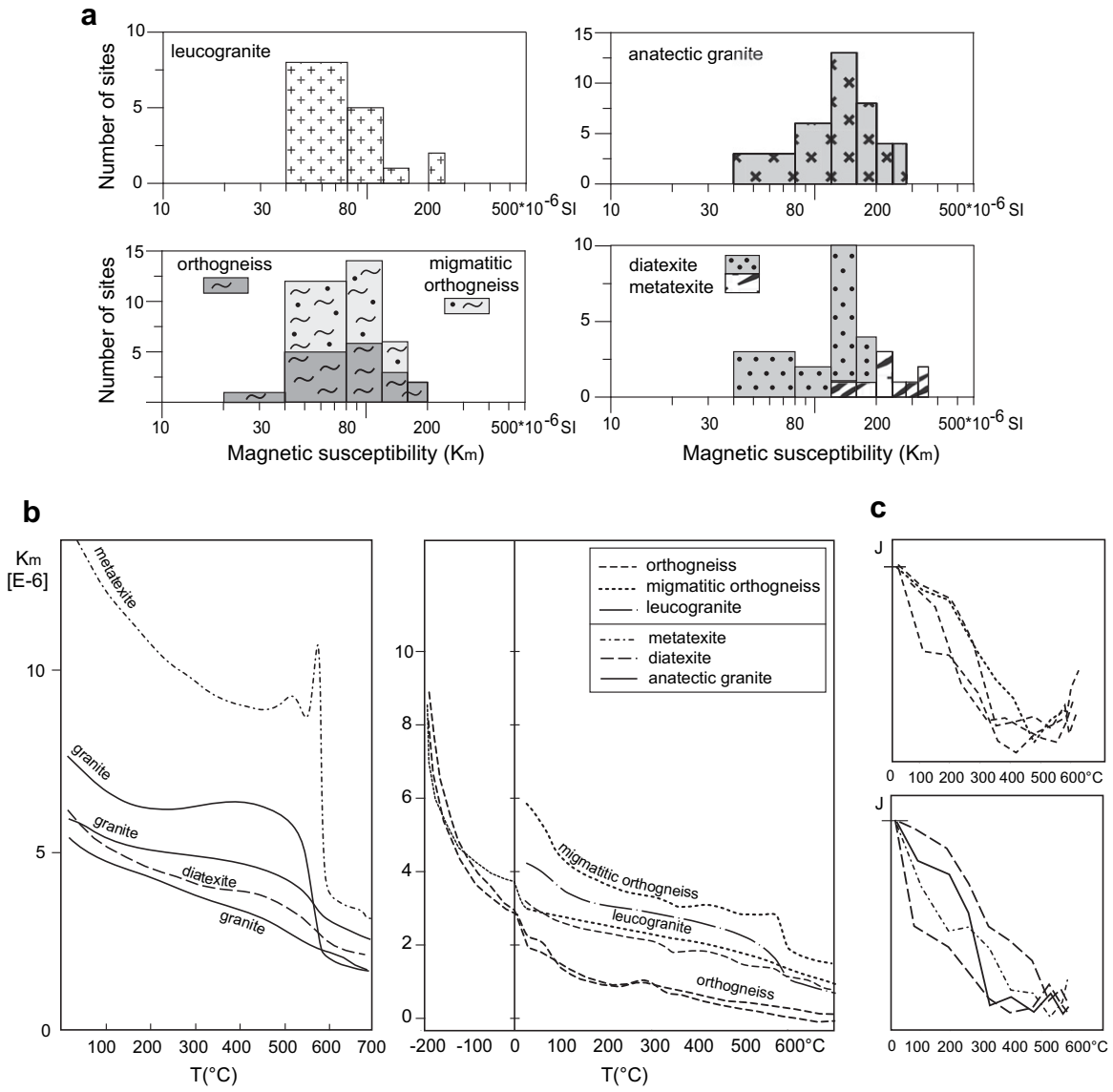

Fig. 6. Magnetic mineralogy data for leucogranites, orthogneiss, migmatitic orthogneiss, anatectic granites, diatexites and metatexites: a) histograms of magnetic susceptibility. b) Magnetic susceptibility versus temperature curves. c) Demagnetization curves of Natural Remanent Magnetization.

of the SOD. In contrast, in the migmatitic orthogneiss the magnetic anisotropy ellipsoids show weakly oblate to prolate shapes and the anisotropy degree is slightly weaker ($P' < 1.07$) than that in the orthogneiss (Fig. 8). The magnetic fabric patterns of the veins of the NOD can be subdivided into two main groups according to their orientations and composition. The first group, the leucogranite veins, is characterized by two sets of sub-vertical magnetic foliations striking NW–SE and NE–SW, containing weakly inclined magnetic lineations and exhibiting oblate to plane shapes of the magnetic ellipsoids (Fig. 8). The second group, the anatectic granite veins, exhibit a dominantly plane fabric and is represented by SE dipping planes which contain a gently S plunging lineation (Fig. 8). Less developed veins show sub-horizontal magnetic foliation and NE trending sub-horizontal lineation.

6. Discussion

In the following we will discuss the bulk flow parameters of the host metasedimentary migmatites and granites controlling complex deformation of the orthogneiss bodies which are regarded as anisotropic inclusions surrounded by these viscous, melt-bearing rocks. The resulting deformation overprints recorded in three zones of orthogneiss domains will be numerically modeled to simulate the variations in shape and degree of anisotropy of the AMS ellipsoid.

6.1. A model of melt proportion-dependent deformation of the migmatitic complex

6.1.1. Kinematic interpretation of the magnetic fabrics in host metasedimentary migmatites and granites

The magnetic fabrics measured in the metasedimentary migmatites and anatectic granites are identical but the anisotropy degree and degree of oblateness decrease with increasing melt proportion (Figs. 7 and 9). The variations of the magnetic fabric and melt proportion during the deformation of partially molten rocks could be explained by the model of strain partitioning suggested by Vigneresse and Tikoff (1999). These authors

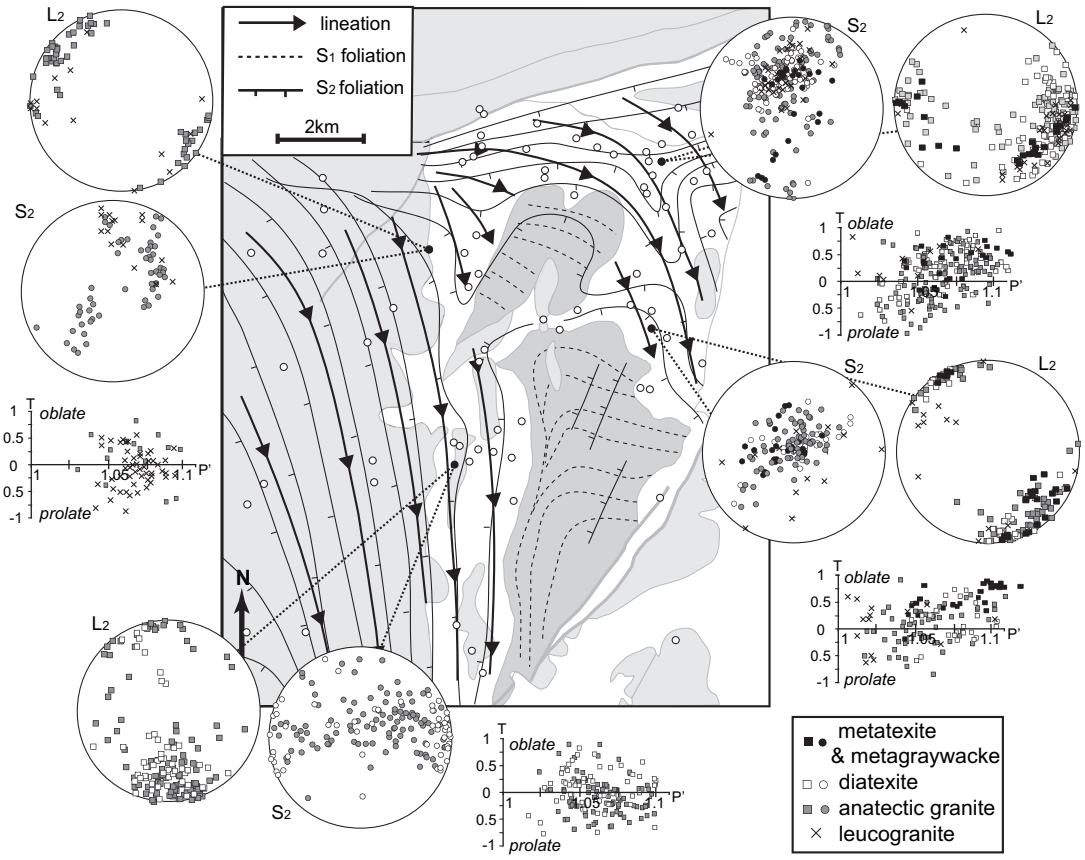

Fig. 7. Synoptic map of the studied area showing the S_1 and S_2–L_2 trajectories with discordant structures between the two orthogneiss bodies and the homogeneous flow pattern of the surrounding diatexites and anatectic granites. Pole diagrams of magnetic foliations and lineations (lower hemisphere projection) and P′–T graphs from metasedimentary migmatites and granites are shown. Magnetic foliations - minimal susceptibility direction (K_3), magnetic lineations - maximum susceptibility direction (K_1) in stereonets.

propose that when the melt escape threshold (Vigneresse et al., 1996) is achieved, the melt segregates into continuous layer, such that the bulk strain partitioned into a coaxial part of the restite and a non-coaxial part in the melt. In such a model the anisotropy degree of the "weakly deformed" restites (metagraywackes boudins in our case) should be lower than that of the "strongly deformed" melt (diatexites and anatectic granites). This is not the case in the studied area where the metagraywacke boudins show highest degree of magnetic susceptibility from all studied rocks and are strongly elongated parallel to the anatectic granite lineation in contrast to the oblate shapes of their magnetic ellipsoids (Fig. 7). This incompatibility suggests that the structural and fabric pattern result from a complex D_1 and D_2 history and cannot be explained by the strain partitioning model of Vigneresse and Tikoff (1999).

The western and eastern domains of the metasedimentary migmatites and anatectic granites can be considered as regions that accommodated the same deformation during melt production and magma flow with increasing proportion of melt towards west (Fig. 5). Our magnetic fabric data also show that from east to west the shape of the magnetic ellipsoid evolves from weakly oblate to plane strain or weakly prolate along with a decrease in the anisotropy degree (Fig. 9). Kinematic indicators suggest that the major D_2 deformation was non-coaxial with a normal component of movement compatible with crustal scale extension in SSE-NNW direction (Kratinová et al., 2007).

This D_2 framework allows estimating the orientations of the instantaneous $(\dot{S}_1, \dot{S}_2, \dot{S}_3)$ and finite (S_1, S_2, S_3) stretching axes (Fig. 10). Assuming, that the S_1, S_2 plane dips generally 20° to the southwest, the stretching S_1 direction plunges 10° to the southeast and the deformation is a sinistral simple shear flow, the instantaneous $\dot{S}_3$ direction can be defined as shown in Fig. 10. Consequently, the instantaneous strain axis $\dot{S}_3$ is deduced to plunge 50° to east and $\dot{S}_1$ to plunge 15° to the north. In the case of combined simple and constrictional pure shear, which is more compatible with weakly prolate magnetic ellipsoid in diatexites and granites, $\dot{S}_3$ will rotate towards the direction of S_3.

6.1.2. *Kinematic interpretation of the magnetic fabrics at low to intermediate melt proportions (centre and internal margin of SOD)*

The AMS fabric of veins in the centre of the SOD (Fig. 8) is compatible with the orientation of the tensile fractures that would be generated for principal shortening directions S_1, S_3 defined previously for the external flow. Fig. 10a shows that the instantaneous stretching axis $\dot{S}_3$ approximately parallels the internal anisotropy of the orthogneiss domain. We therefore suggest that the leucogranite veins in the central part of orthogneiss body originated as a result of interfolial dilation by the principal compressive stress being oriented sub-parallel to the mechanical anisotropy, similar to that described by Barraud et al. (2004). The AMS also shows that the leucogranite flowed parallel to the S_1 planar anisotropy of the host orthogneiss in the direction of D_2 stretching.

Magnetic fabric orientations in the orthogneiss of the internal margin of the SOD are compatible with the rotation of the S_1 gneissosity as a result of buckling of the originally east–west trending steep mechanical anisotropy into folds with wavelengths on the order of 100 m (Fig. 4). The intersections of the magnetic foliations from the different parts of orthogneiss domain plunge to the SSW or to the W at angles less than 40–50° and coincide with the hinges of the large scale folds (Fig. 8). We argue that the folding

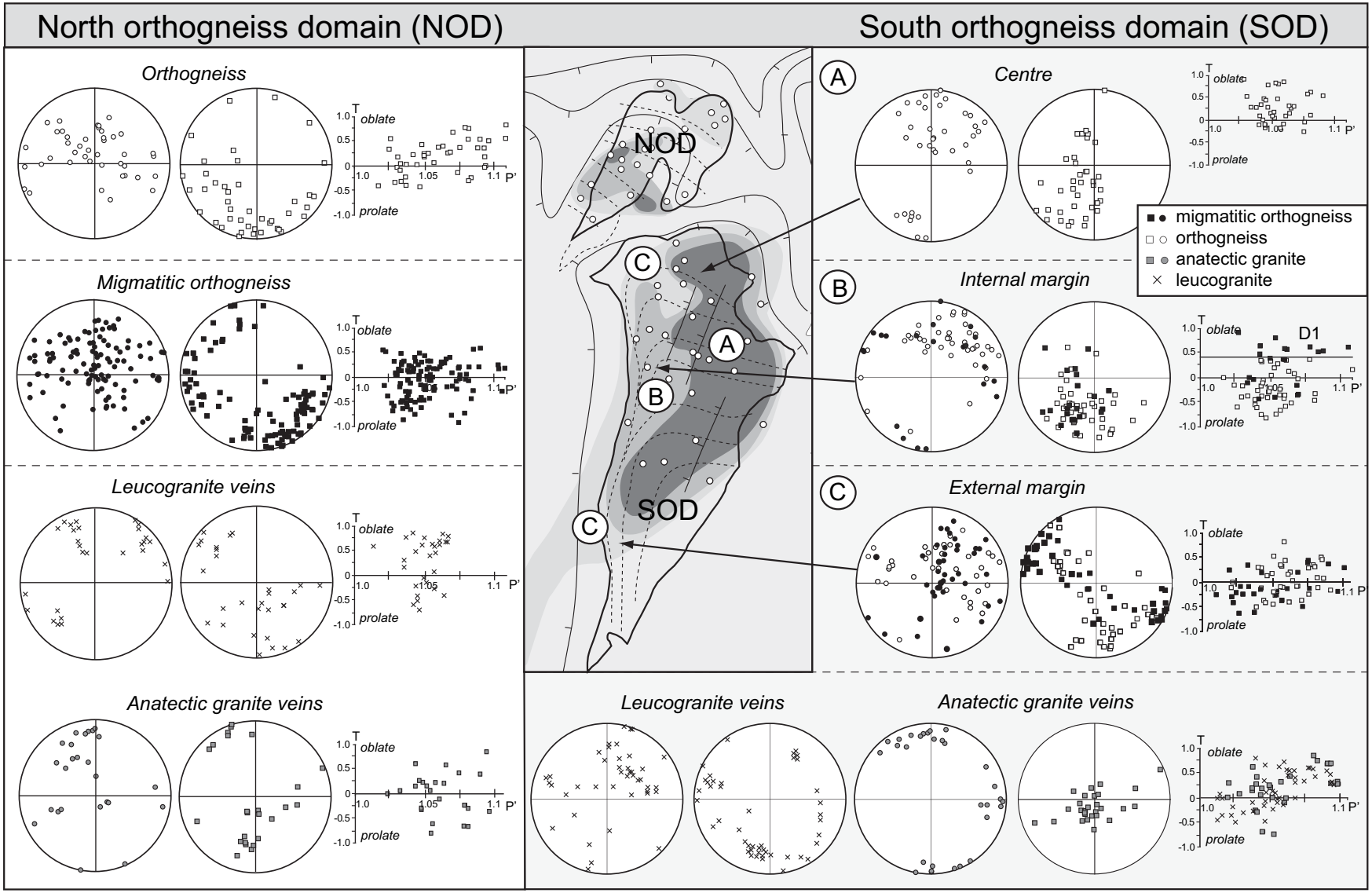

Fig. 8. Pole diagrams of magnetic foliations (circle) and lineations (square) (lower hemisphere projection) and P′–*T* graphs from both orthogneiss domains (SOD and NOD). In both orthogneiss domains the data for orthogneiss (white circle/square) and migmatitic orthogneiss (black circle/square), leucogranite veins (cross) and granite veins (grey circle/square) are shown separately. In the internal margin of SOD data corresponding to the orientations characteristic for central zone of the SOD are emphasized (dark grey symbols).

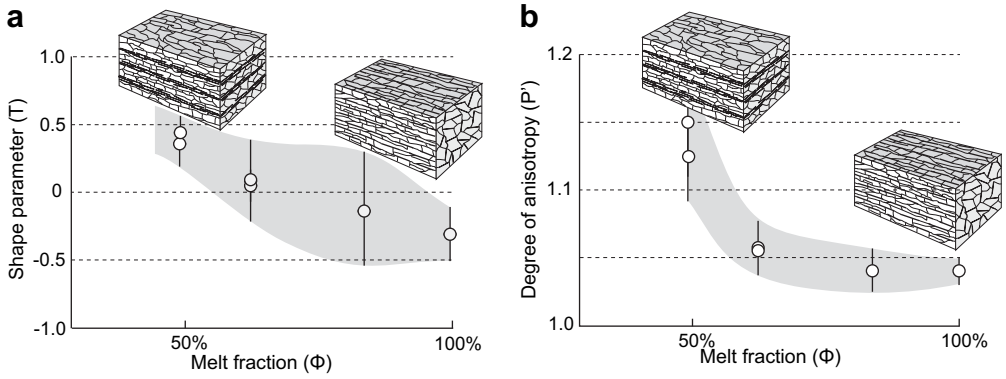

Fig. 9. Relationship between melt proportion and fabric elements in the metasedimentary migmatites: (a) Development of the shape parameter (T) with increasing melt proportion. (b) Development of the degree of magnetic anisotropy (P') with increasing melt proportion.

of the orthogneiss foliation was easy to initiate because of the favorable orientation of the mechanical anisotropy with respect to the S_3 direction. An example of these large scale folds with interlimb angles of 90° and with axial planes parallel to the external S_1S_3 plane of the magmatic flow is given in Fig. 10a. We observe that magnetic lineations are rotated together with the foliation planes around the fold hinge and, when represented on a stereoplot, they are found to lie on a small circle. This indicates that the folding was governed by active amplification, namely by flexural slip folding without any contribution of post-buckle flattening. Post-buckle flattening would rotate the lineations in such a manner that they would tend to lie on a great circle. With continued deformation the folds tightened with interlimb angles of ~30°, the axial planes became close to the external granite flow plane and the hinges rotated towards the direction of the regional stretching (Fig. 10b). The lineations are still distributed along small circles suggesting that active buckling rather than flattening dominated up to high strains.

Our study shows, that with an increasing melt fraction the anisotropic rock compressed parallel to layering significantly weakens and that the melt-solid rock multilayer starts to buckle. Such an active amplification of large scale folds points to a high mechanical anisotropy and/or a strong viscosity contrast between melt and rock (Fig. 4). The fabric of the folded domain becomes discordant to that of the migmatitic orthogneiss whose orientation, anisotropy degree and shape parameter coincides with the fabric of the surrounding granites (Figs. 4 and 8). This fabric behavior of the migmatitic orthogneiss is similar to that of the axial plane leucosomes, as shown by Vernon & Paterson (2001). The axial planar orientation of the magnetic foliation and the orientation of the magnetic lineation with respect to the geometry of the open and closed folds (Fig. 10) suggest that these fabric elements are completely transposed with respect of the original orthogneiss fabric.

6.1.3. Kinematic interpretation of the magnetic fabric at high melt fractions (external margin of the SOD and the NOD)

We suggest that orthogneisses formed a layered system in which the orientation of the layering was sub-parallel to the general flow direction of the surrounding and interlayered granites and metasedimentary migmatites. This interpretation is supported by the presence of recumbent, often rootless folds (Fig. 2a), suggesting that the whole system was an isoclinally folded migmatite-orthogneiss multilayer with fold hinges rotated into direction of regional stretching. Ongoing shortening and an increase in the melt fraction further weakened the melt-solid rock multilayer which progressively developed a marked planar anisotropy perpendicular to the main shortening direction. Because of vertical shortening, the process of extension induces a sub-horizontal planar anisotropy in the felsic orthogneiss (Fig. 4). Layer perpendicular shortening of layered rocks develops pinch-and-swell structures in the relatively competent layers and conjugate normal kink bands (extensional shears) in the mechanically anisotropic matrix (Kidan and Cosgrove, 1996).

Accordingly the leucogranite veins oriented at low angles to the main anisotropy of the gneiss-migmatite multilayer (Fig. 4) are interpreted as conjugate normal kink bands or extensional shears filled by granitic magma (Cosgrove, 1997). The orientations of the magnetic lineations (Fig. 8) suggest that the extensional shears developed in the same kinematic framework as the main foliation, i.e. vertical shortening and SE-NW extension. The general oblateness of the magnetic ellipsoids (Fig. 8) corresponds to the combined pure and simple shear that operated during movement along shears and their filling by melt. The geometrical relationship observed between the leucogranite veins and the fabric of both orthogneiss types multilayers, is fully compatible with the model of shear band development during layer perpendicular shortening of a highly anisotropic multilayer (Kidan and Cosgrove, 1996). The implication of the normal kink bands and the other structures discussed above is that the rocks of the external margin of the SOD and the bulk of the NOD were highly anisotropic during their deformation and that these partially molten orthogneisses contained units with highly different strengths, i.e. less competent migmatitic orthogneiss and granites and competent orthogneiss.

7. A numerical model for the polyphase magnetic fabrics

Numerical modeling was used to determine whether it was possible to develop the observed prolate fabrics of the orthogneiss in the internal margin of the SOD and the oblate fabrics in the outer margin of the SOD and NOD by an extensional deformation (D_2) superimposed on a previous plane strain or oblate fabric. We used the software of Ježek and Hrouda (2002). As shown by magnetic mineralogy study the magnetic carriers in the modeled orthogneiss were biotite grains with highly oblate shapes of aspect ratio 5, with a shape magnetic anisotropy and a magnetic intensity $P' = 1.3$ (Martín-Hernández and Hirt, 2003).

The early deformation D_1 was modeled by reorienting the initial isotropic grain population through plane strain or axial flattening. This generates a fabric comparable to that observed in the central part of the SOD (Fig. 8). D_2 was then superposed onto D_1 as a weak constrictional deformation derived from the magnetic fabrics observed in the anatectic granites. As mentioned earlier, this deformation regime is considered to characterize the regional extension D_2. A range of different mutual orientations of D_1 and D_2 in

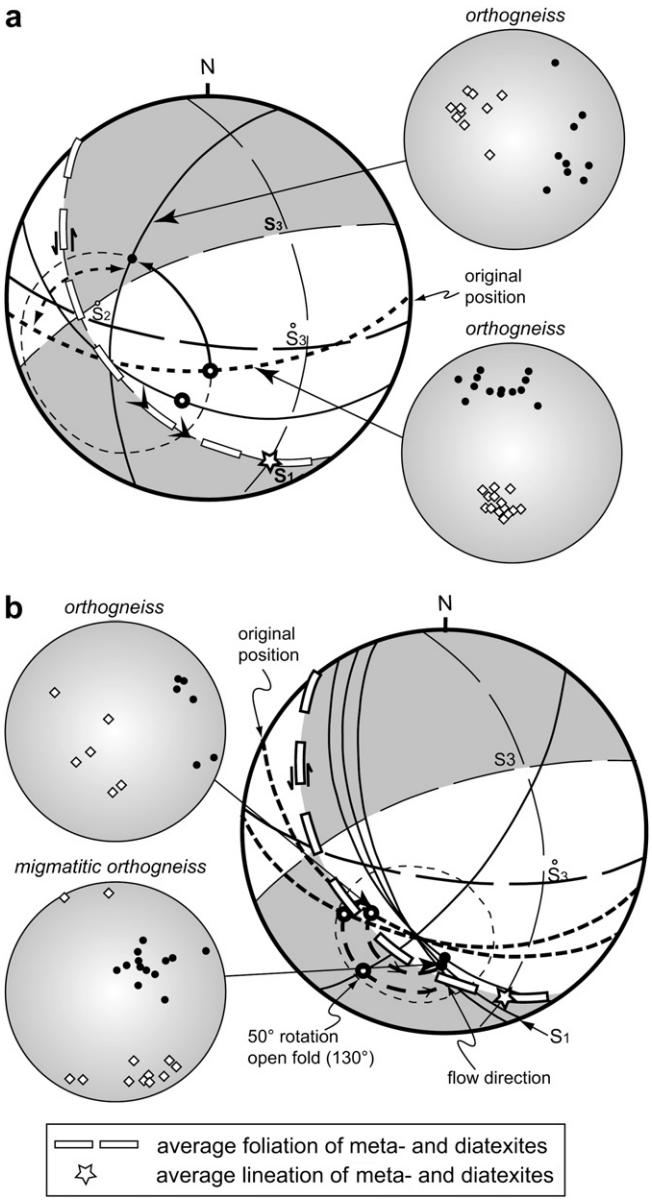

Fig. 10. Orientation diagrams showing the relationship between the external migmatite flow and the fabric within (a) the internal and (b) the external SOD margin. The diagram is separated into extension (dark) and shortening (white) sectors of instantaneous strain for sinistral simple shear. The thin dashed line bisecting the shortening sector represents the S_2 and S_3 plane of instantaneous D_2 deformation. The two thin full curves represent the rotated limbs of the large fold and the circles represents the rotated lineations (open circle for the original position and black circle for the finite position). (b) The rotated foliations are close to the main flow plane (white dashed curve) and the fold axes (intersection of planes) rotate towards the direction of the regional stretching (white star).

association with the large scale buckling of the S_1 fabric was considered, and deformation overprints in the locked short limbs of the large scale folds (layer parallel shortening) and in the highly rotated long limbs (layer perpendicular shortening) were examined.

Four examples are shown (Fig. 11) in which numerical modeling reproduces the fabrics observed in the internal and external margins of the SOD margin and in the NOD. Fig. 11a shows the P′–T graphs during the development of the different fabrics. Steps, marked on the graph in Fig. 11a, of fabric development are illustrated in Fig. 11b by the equal area projections of the biotite. Case A shows the fabric development of D_2 from an originally isotropic biotite orientation towards a weakly prolate geometry in the range of the observed P′ values of around 1.05 (Figs. 7 and 8). The deformation that created this fabric was then used to overprint different D_1 fabrics illustrated in cases B to E. In case B, D_1 was chosen so in order to cause a vertical lineation parallel to the D_2 shortening direction (open square in Fig. 11b). Such an orthogonal superimposition of two plane strains produces P′ and T parameters in the range of the observed values in the internal margin of the SOD (Fig. 8). The P′–T path evolves towards oblateness during the first strain increments followed by prolateness with increasing deformation (Fig. 11a curve B). Case C considers D_1 and D_2 fabric ellipsoids similar to the previous case B but with an initial L_1 horizontal lineation. In contrast to case B, the P′-T trajectory is towards prolateness followed by the development of plane strain fabrics at high strain intensities. Case D represents the superimposition of D_2 on a vertically oriented oblate fabric. The result is a rapid evolution towards prolateness for a minimum change in the anisotropy degree, followed by a weakly prolate fabric. The results modeled by case E illustrate a case in which a low angle exists between the D_2 shortening axis and the pole to S_1, while L_1 and the D_2 stretching direction initially formed a relatively high angle. The resulting P′–T trajectory remains oblate for the whole D_2 deformation history.

Because of the variable dips of S_1 in the centre of the SOD (Fig. 8) and the high angle between S_1 and the shortening in the NOD we have modeled the influence of the dip angle on the P′–T trajectory of $D_1 + D_2$. Numerical simulations revealed high sensitivity to the resulting fabric on the orientation of D_2 with respect to D_1. Fig 12 shows that prolate fabrics can be produced only if S_1 is at a high angle ($>70°$) to the D_2 shortening direction.

The numerical simulations produce oblate to a plane strain magnetic fabrics in the core of the SOD whereas the internal margin of the SOD the fabrics are dominantly prolate and subordinately oblate. Another result is that the sub-horizontal shortening of the original plane strain or oblate vertical S_1 foliation may result in prolate $D_1 + D_2$ fabrics. This agrees with the proposed strain history involving large scale folding and the progressive shortening of the short limbs of the asymmetrical folds rotated toward the shortening axis. Such a deformation may occur either via homogeneous shortening of the short limbs or by the development of an incipient cleavage. Whatever the deformation mechanism, the resultant prolate fabric will develop either a "true" stretching lineation or an intersection lineation. These possibilities cannot be distinguished from each other using the AMS technique but the most likely mechanism is a combination of passive reorientation and dynamic recrystallization of the micas, as supported by the experimental fabric studies (Nicolas and Poirier, 1976). These studies showed that at high temperatures dynamic recrystallization favors an intense fabric development along the path predicted by the passive marker model of March (1932) even if the role of the initial preferred orientation in such a process is unclear. The combination of dynamic recrystallization and passive reorientation of biotite can be also accompanied with melt-assisted grain boundary sliding of matrix minerals (Hasalová et al., 2008a).

Finally, the predominance of oblate fabrics in the external SOD margin and in the NOD can be explained by the numerical simulation. Case E of Fig. 11 and the associated oblate P′–T paths of Fig. 12 show that a low angle between the D_2 shortening axis and the pole to S_1 leads to oblate fabrics for whatever the type of the pre- D_2 deformation fabric ellipsoid. It is therefore proposed that these oblate fabrics reflect shortening at a high angle to the limbs of large folds (Fig. 10), typical for a mechanism of post-buckle flattening.

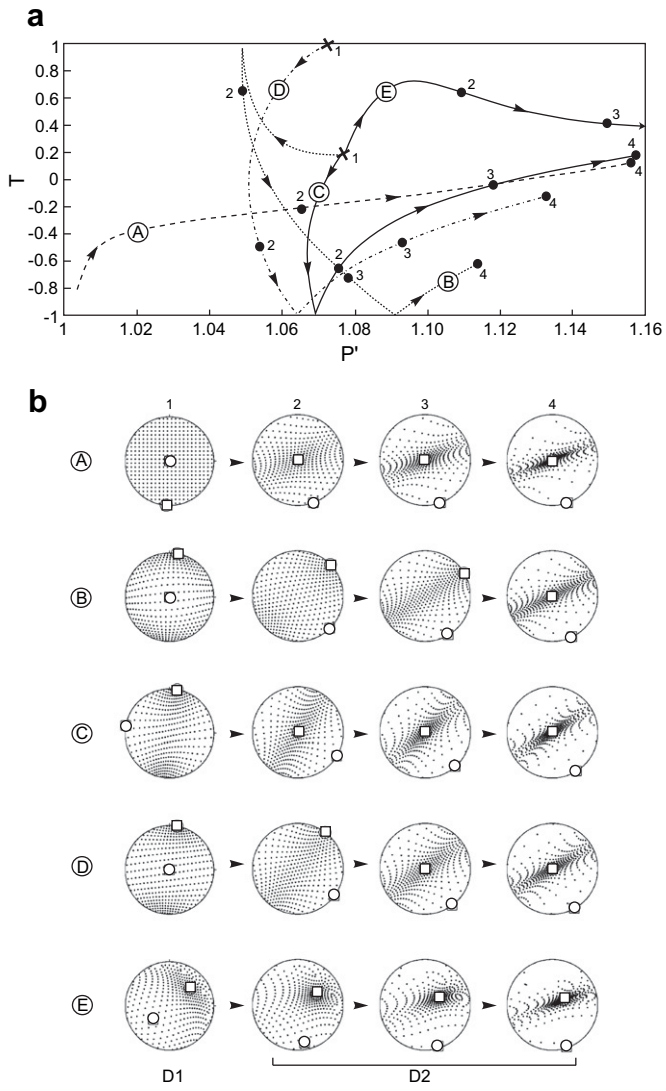

Fig. 11. Results of numerical simulation of AMS superposition shown in P′–*T* space (a) and stereonet (b). The stereonets correspond to the marked dots on the P′–*T* path. The black cross represents the initial step. Case A represents the D_2 deformation superposed on uniformly distributed biotites and showing D_2 fabric development in anatectic granites. In this case the initial step is isotropic. The constriction components of the velocity gradient tensor are characterized by the ratio 1:4 for intermediate and short axes, respectively. Case B shows the nearly orthogonal superposition of the D_2 plane strain deformation onto the D_1 plane strain fabric. Case C has similar D_1 and D_2 fabric ellipsoids as Case B but the L_1 lineation horizontal. Case D shows the superposition of the D_2 plane strain deformation on a vertically oriented oblate D_1 fabric. Case E considers the superposition of the D_2 deformation onto the D_1 fabric for a low angle between the D_2 shortening axis and the pole to the S_1 foliation. In cases B–E initial steps are D_1. The pole to the AMS foliation (open circle) and the lineation (open square) are indicated.

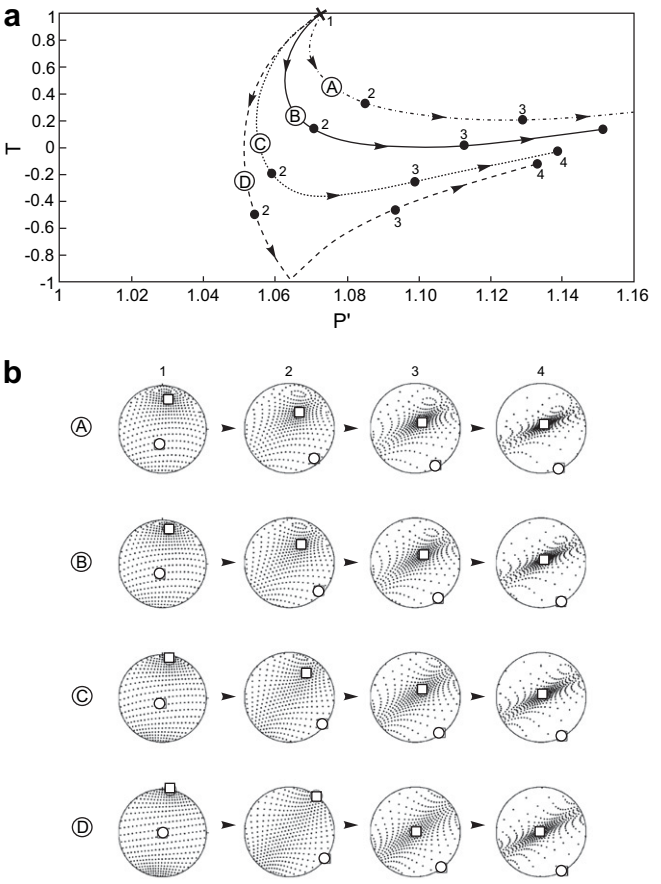

Fig. 12. Numerical simulations documenting the sensitivity of the developed fabric to the relative orientations of the D_1 and D_2 deformations. The variations of D_1 fabric orientations are expressed in dip values ranging from 60° (curve D) to 90° (curve A). The curve D coincides with the case D of the Fig. 11. The pole to the AMS foliation (open circle) and the lineation (open square) are indicated.

8. Origin of migmatitic orthogneiss mineralogy and AMS fabric

The remaining problem is the explanation of the weakly to moderately prolate fabrics in the migmatitic orthogneiss. As these fabrics are developed either at a high angle to S_1 in the external SOD margin or parallel to S_1 in the NOD, their symmetry cannot be explained by fabric overprints like in the previous section.

The topology of the new feldspars and quartz in migmatitic orthogneiss indicates that they crystallized from a former melt (Sawyer, 1999) and biotite and feldspars resorption indicates a disequilibrium reaction with the melt (Büsch et al., 1974). Slight increase of X_{Mg} and Ti content in the biotite indicate that this event took place at slightly higher temperatures compared to the orthogneiss formation. Importantly, the migmatitic orthogneiss reveals crystallization of magnetic accessory phases (titanomagnetite) which is incompatible with in-situ partial melting model of felsic orthogneiss because of obvious lack of Ti content in this rock. Therefore, the crystallization of titanomagnetite but also of other minerals like albite overgrowths, new K-feldspar and quartz grains, could reflect an external source of the melt (Hasalová et al., 2008a,b). It is likely that surrounding metasedimentary migmatites, because of their composition and high content of Ti–Fe bearing phases, represent sources of melt infiltrating into progressively deforming orthogneiss bodies.

The deformation of migmatitic orthogneiss is marked by complete mixing and randomization of biotite in the matrix, reduction in the aspect ratio of biotite and its compositional changes associated with a complete reworking and resetting of the original aggregate structure of the orthogneiss. Thus the bulk deformation mechanisms in these migmatitic orthogneiss may be significantly different from those operating in orthogneiss and in surrounding granites. The most likely mechanisms are a passive rotation of biotite and titanomagnetite grains during independent particulate flow accommodated by melt enhanced grain boundary sliding (Paterson, 2001; Borradaile and Jackson, 2004). Therefore the AMS fabric originated as a result of D_2 flow and can be modeled

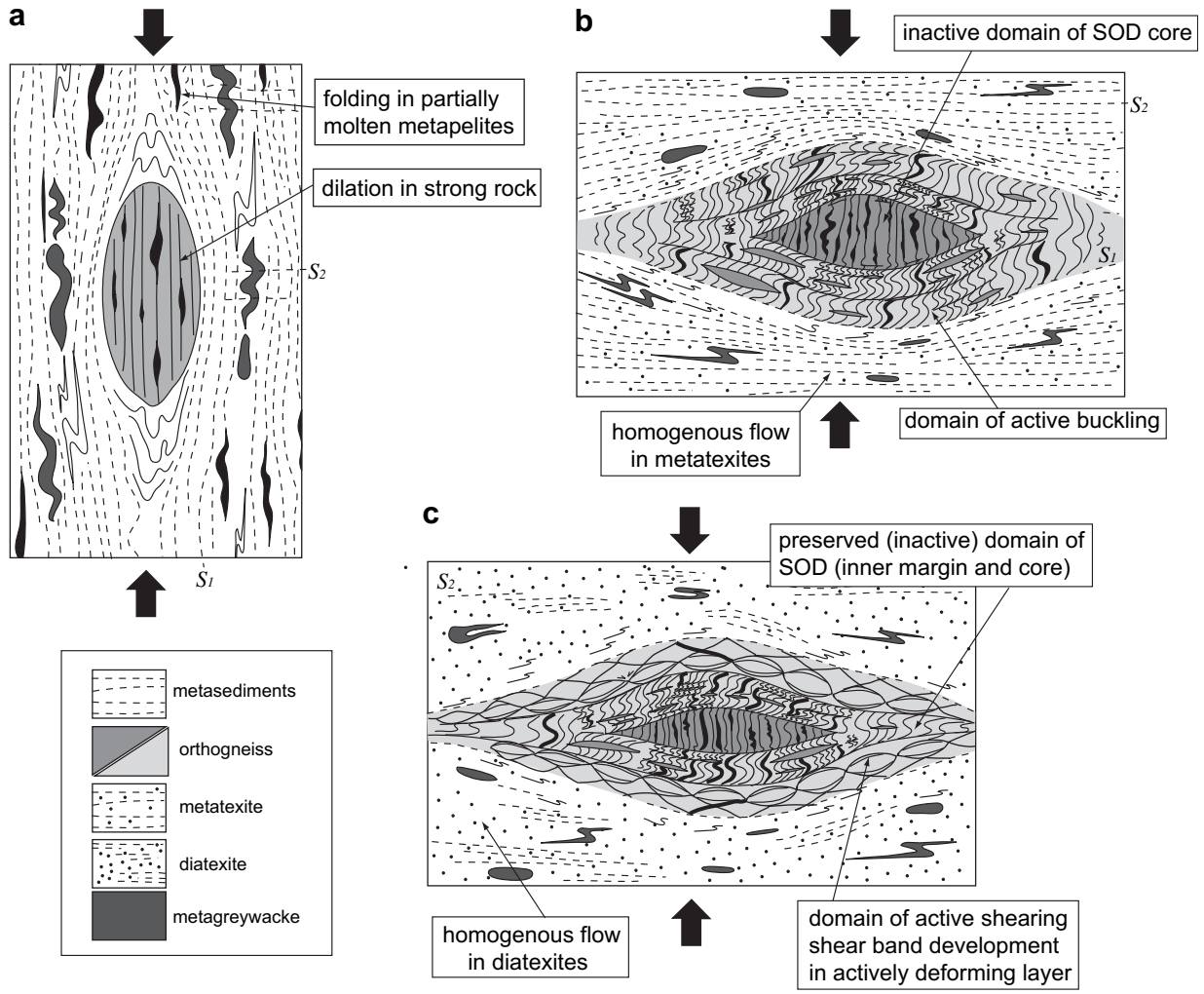

Fig. 13. Three stages of the mechanical and rheological evolution of orthogneiss bodies and host metasedimentary migmatites: (a) Early stage of layer parallel shortening. (b) Later stage in the deformation when the margin of the orthogneiss body has been transformed to an orthogneiss/granite multilayer. (c) In the final stage further homogeneous deformation of host diatexites is accompanied by flattening and intensification of the orthogneiss fabric.

only for complex magnetic mineralogy including both biotite and titanomagnetite.

9. Rheological considerations

In the proposed kinematic model, the two orthogneiss domains are considered as two giant anisotropic inclusions immersed in homogeneously flowing metasedimentary migmatites and granites (Figs. 4 and 13). Because the internal parts of the orthogneiss domains preserved their original solid state fabrics and foliation-parallel veins we assume that the anisotropy parallel dilation of the cores of the orthogneiss likely occurred when the whole system was strong and contained only a relatively small amount of melt (Fig. 13a).

In contrast the buckling of the orthogneiss-melt multilayer took place when the surrounding metasediments became more molten (metatexite stage) but were still capable of transmitting the contractional stress across the whole metasedimentary and orthogneiss domain. Layer parallel shortening in the internal SOD margin lead to the reorientation of magnetic minerals documented by the development of prolate fabrics in the orthogneiss. At this stage the deformation affected only highly molten margins of the otherwise rigid orthogneiss domains, thus preserving original fabrics in the core of the SOD (Fig. 13b).

With ongoing shortening and melting the relic solid state layers in the isoclinally folded orthogneiss-melt multilayer became perpendicular to the bulk contraction and further homogeneous shortening produced oblate strains in the orthogneiss. Increased melting of the host rock probably increased the rheological contrast between the surrounding anatectic granites and the orthogneiss domains that become relatively rigid and almost undeformable. It is only the external margin of the SOD and the whole NOD that experienced continuous deformation similar to the adjacent homogeneously deforming migmatites and granites, while the core and internal margin of the SOD remained relatively stiff (Fig. 13c).

Acknowledgements

This work was financially supported by the UMR 7516-7517 grants of CNRS and Université Louis Pasteur in Strasbourg, the French National Agency (No. 06-1148784 to K. Schulmann) and the Ministry of Education of the Czech Republic (No. MSM0021620855 to J. Ježek). Visits by P. Hasalová to ULP Strasbourg were funded by the French Government Foundation (BGF). We would like to thanks J.L. Bouchez and other anonymous reviewer for their constructive reviews and the journal editor T. Blenkinsop for all his editorial work on this manuscript.

References

Barraud, J., Gardien, V., Allemand, P., Grandjean, P., 2004. Analogue models of melt-flow networks in folding migmatites. Journal of Structural Geology 26, 307–324.

Benn, K., 1994. Overprinting of magnetic fabrics in granites by small strains: numerical modeling. Tectonophysics 233, 153–162.

Borradaile, G.J., Henry, B., 1997. Tectonic applications of magnetic susceptibility and its anisotropy. Earth-Science Reviews 42, 49–93.

Borradaile, G.J., Jackson, M., 2004. Anisotropy of magnetic susceptibility (AMS): magnetic petrofabrics of deformed rocks. In: Martin-Hernandez, F., Lünenburg, C.M., Aubourg, C., Jackson, M. (Eds.), Magnetic Fabric: Methods and Applications, vol. 238. Geological Society London, Special Publication, pp. 299–360.

Bouchez, J.L., 1997. Granite is never isotropic: an introduction to AMS studies of granitic rocks. In: Bouchez, J.L., Hutton, D.H.W., Stephens, W.E. (Eds.), Granite: from Segregation of Melt to Emplacement Fabrics. Kluwer Academic Publishers, Dordrecht, pp. 5–112.

Brown, M., Averkin, Y., McLellan, E.L., Sawyer, E.W., 1995. Melt segregation in migmatites. Journal of Geophysical Research 100, 15655–15679.

Büsch, W., Schneider, G., Mehnert, K.R., 1974. Initial melting at grain boundaries. Part II: melting in rocks of granodioritic, quartz dioritic and tonalitic composition. Neues Jahrbuch für Mineralogie Monatshefte 8, 345–370.

Cosgrove, J.W., 1997. The influence of mechanical anisotropy on the behaviour of the lower crust. Tectonophysics 280, 1–14.

Debacker, T.N., Robion, P., Sintubin, M., 2004. The anisotropy of magnetic susceptibility (AMS) in low-grade, cleaved pelitic rocks: influence of cleavage/bedding angle and type and relative orientation of magnetic carriers. In: Martín-Hernández, F., Lünenburg, C.M., Aubourg, C., Jackson, M. (Eds.), Magnetic Fabric: Methods and Applications, vol. 238. Geological Society London, Special Publications, pp. 77–107.

Egydio-Silva, M., Vauchez, A., Raposoa, M.I.B., Bascou, J., Uhleind, A., 2005. Deformation regime variations in an arcuate transpressional orogen (Ribeira belt, SE Brazil) imaged by anisotropy of magnetic susceptibility in granulites. Journal of Structural Geology 27, 1750–1764.

Ferré, E.C., Teyssier, C., Jackson, M., Thill, J.W., Rainey, E.S.G., 2003. Magnetic susceptibility anisotropy: a new petrofabric tool in migmatites. Journal of Geophysical Research B: Solid Earth 108 EPM 5-1-5-14.

Hasalová, P., Schulmann, K., Lexa, O., Štípská, P., Hrouda, F., Ulrich, S., Haloda, J., Týcová, P., 2008a. Origin of migmatites by deformation-enhanced melt infiltration of orthogneiss: a new model based on quantitative microstructural analysis. Journal of Metamorphic Geology 26, 29–53.

Hasalová, P., Štípská, P., Powell, R., Schulmann, K., Janoušek, V., Lexa, O., 2008b. Transforming mylonitic metagranite by open-system interactions during melt flow. Journal of Metamorphic Geology 26, 55–80.

Housen, B.A., Richter, C., Van der Pluijm, B.A., 1993. Composite magnetic anisotropy fabrics: experiments, numerical models, and implications for the quantification of rock fabrics. Tectonophysics 220, 1–12.

Hrouda, F., 1991. Models of magnetic anisotropy variations in sedimentary thrust sheets. Tectonophysics 185, 203–210.

Jelínek, V., 1978. Statistical processing of anisotropy of magnetic susceptibility measured on groups of specimens. Studia geophysica et geodaetica 22, 50–62.

Jelínek, V., 1981. Characterization of the magnetic fabric of rocks. Tectonophysics 79, 63–67.

Ježek, J., Hrouda, F., 2002. Software for modeling the magnetic anisotropy of strained rocks. Computers and Geosciences 28, 1061–1068.

Kidan, T.W., Cosgrove, J.W., 1996. The deformation of multilayers by layer-normal compression; an experimental investigation. Journal of Structural Geology 18, 461–474.

Kratinová, Z., Schulmann, K., Edel, J., Ježek, J., Schaltegger, U., 2007. Model of successive granite sheet emplacement in transtensional setting: integrated microstructural and anisotropy of magnetic susceptibility study. Tectonics 26, TC6003.

Latouche, L., Fabries, J., Guiraud, M., 1992. Retrograde evolution in the Central Vosges mountains (north-eastern France): implications for the metamorphic history of high-grade rocks during the Variscan orogeny. Tectonophysics 205, 387–407.

March, A., 1932. Mathematische Theorie der Regelung nach der Korngestalt bei Affiner Deformation. Zeitschrift für Kristallographie 81, 285–298.

Martín-Hernández, F., Hirt, A.M., 2003. Paramagnetic anisotropy of magnetic susceptibility in biotite, muscovite and chlorite single crystals. Tectonophysics 367, 13–28.

Nicolas, A., Poirier, J.P., 1976. Crystalline Plasticity and Solid State Flow in Metamorphic Rocks. Wiley Inter Science Edition, London.

Parés, J.M., Van der Pluijm, B.A., 2003. Magnetic fabrics and strain in pencil structures of the Knobs formation, Valley and Ridge Province, US Appalachians. Journal of Structural Geology 25, 1349–1358.

Paterson, M.S., 2001. A granular flow theory for the deformation of partially molten rock. Tectonophysics 335, 51–61.

Rey, P., Burg, J.P., Caron, J.M., 1992. Middle and late Carboniferous extension in the Variscan Belt: structural and petrological evidences from Vosges Massif (Eastern France). Geodinamica Acta 5, 17–36.

Sawyer, E.W., 1999. Criteria for the recognition of partial melting. Physics and Chemistry of the Earth 24, 269–279.

Schaltegger, U., Fanning, C.M., Günther, D., Maurin, J.C., Schulmann, K., Gebauer, D., 1999. Growth, annealing and recrystallization of zircon and preservation of monazite in high-grade metamorphism: conventional and in situ U–Pb isotope, cathodoluminiscence and microchemical evidence. Contributions to Mineralogy and Petrology 134, 186–201.

Schulmann, K., Schaltegger, U., Ježek, J., Thompson, A.B., Edel, J.B., 2002. Rapid burial and exhumation during orogeny: thickening and synconvergent exhumation of thermally weakened and thinned crust (Variscan orogen in Western Europe). American Journal of Sciences 302, 856–879.

Vanderhaeghe, O., 1999. Pervasive melt migration from migmatites to leucogranite in the Shuswap metamorphic core complex, Canada: control of regional deformation. Tectonophysics 312, 35–55.

Vernon, R.H., Paterson, S.R., 2001. Axial-surface leucosomes in anatectic migmatites. Tectonophysics 335, 183–192.

Vigneresse, J.L., Barbey, P., Cuney, M., 1996. Rheological transitions during partial melting and crystallization with application to felsic magma segregation and transfer. Journal of Petrology 37, 1579–1600.

Vigneresse, J.L., Tikoff, B., 1999. Strain partitioning during partial melting and crystallizing felsic magmas. Tectonophysics 312, 117–132.